Supporting Information

Triple Functionalization of Carved N-doped Carbon Nanoboxes with Synergistic Tri-metallic Sulfide for High Performance Lithium-Sulfur Batteries

Yen-Ju Wu, Cheng-Hao Chen, Shin-Hong Lin, Chun-Lung Huang, Yong-Xian Yeh, Jia-Yu Tan, Jing-Ting Su, Cheng-Ting Hsieh, and Shih-Yuan Lu*

Department of Chemical Engineering, National Tsing Hua University, Hsinchu 30013, Taiwan, ROC.

*Email: sylu@mx.nthu.edu.tw

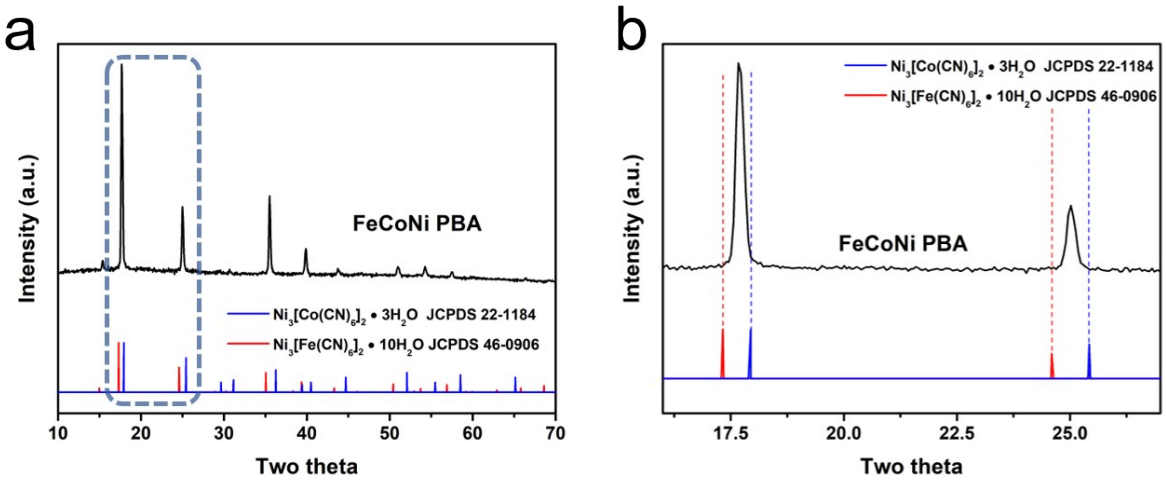

Figure S1. (a) XRD pattern of FeCoNi PBA, (b) locally enlarged XRD pattern.

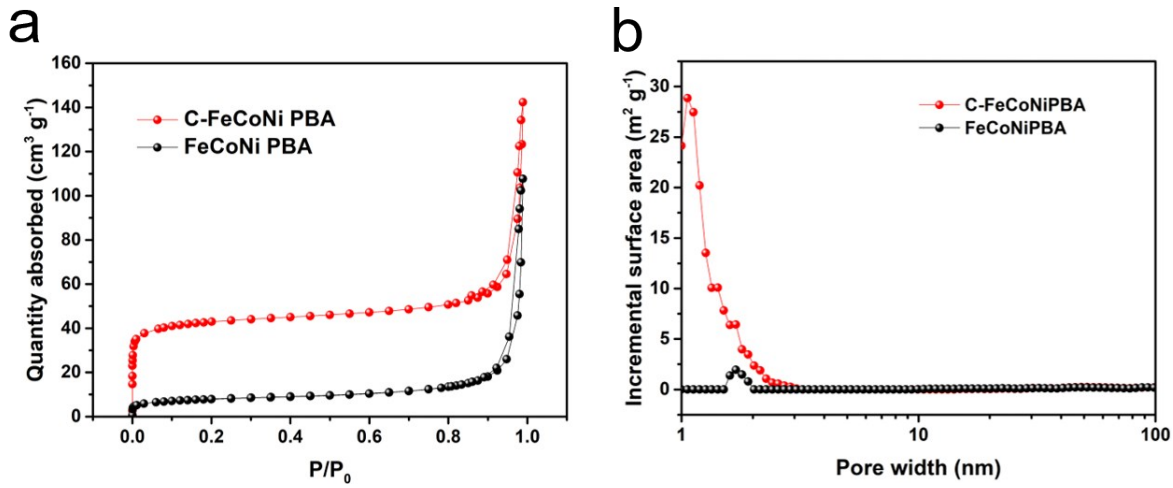

Figure S2. (a) N_2 adsorption/desorption isotherms and (b) incremental pore size distributions of C-FeCoNi PBA and FeCoNi PBA.

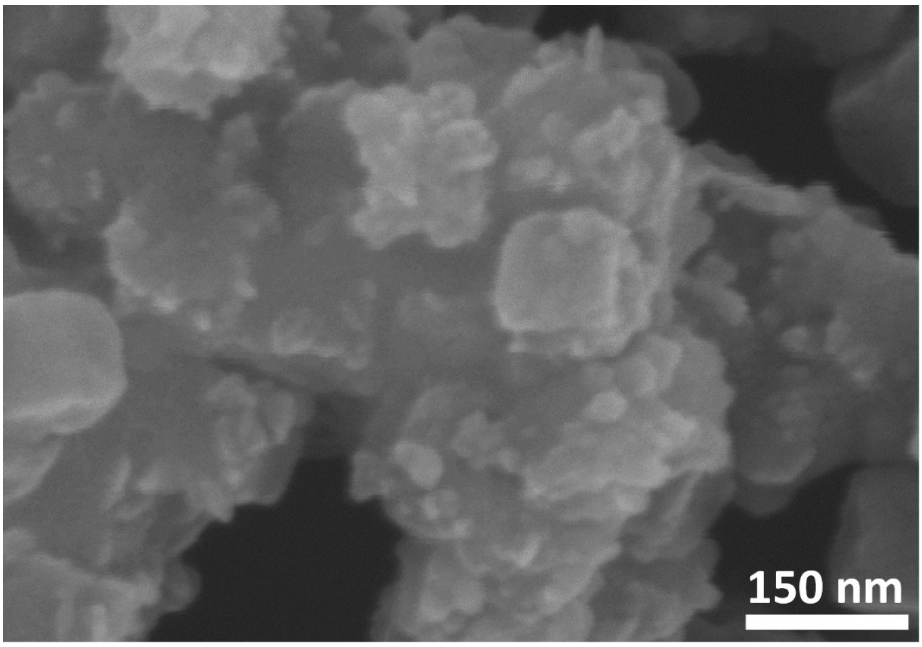

Figure S3. SEM image of S-FeCoNi@C-CNB without coating of PDA.

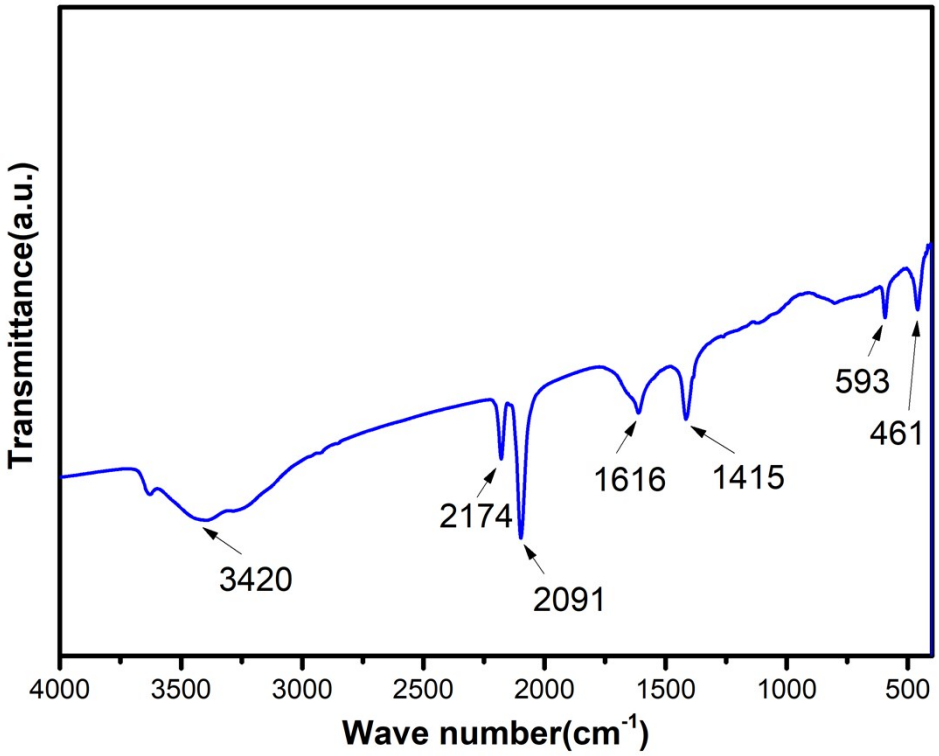

Figure S4. FT-IR spectrum of C-FeCoNi PBA@PDA.

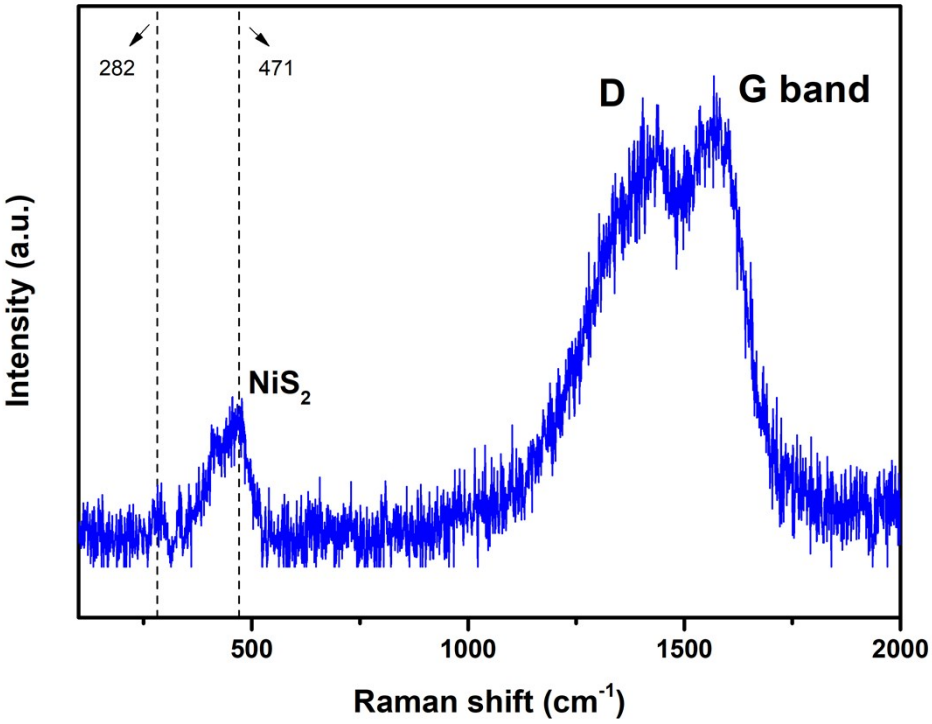

Figure S5. Raman spectrum of S-FeCoNi@C-CNB.

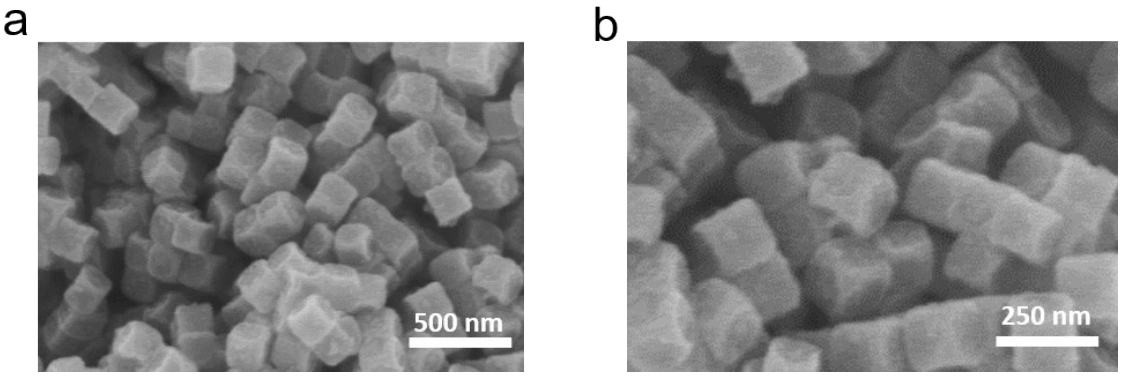

Figure S6. (a) Low and (b) high magnification SEM images of S-FeCoNi@CNB.

Table S1. Specific surface areas and specific pore volumes of characterized samples.

sample	Specific surface area (m^2 g^{-1})	Total pore volume (cm^3 g^{-1})	t-plot micropore volume (cm^3 g^{-1})
FeCoNi PBA	26.8	0.17	0.0038
C-FeCoNi PBA	138	0.22	0.047
C-FeCoNi PBA@PDA	120	0.22	0.034
S-FeCoNi@C-CNB	96.1	0.34	0.0041
S-FeCoNi@CNB	49.4	0.13	0.0016

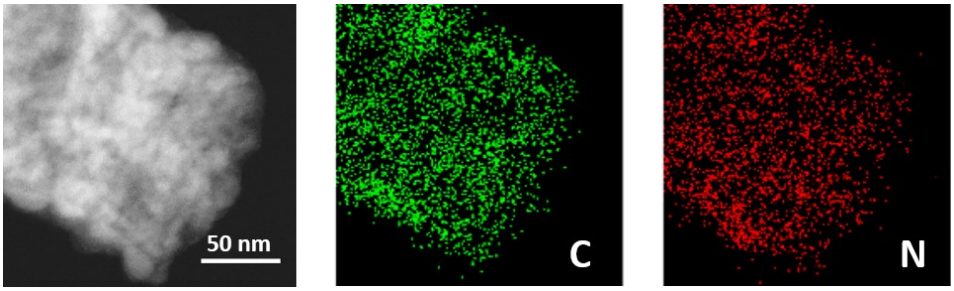

Figure S7. TEM-EDS elemental mapping of C and N in S-FeCoNi@C-CNB.

Table S2. Atomic percentages of constituent elements of S-FeCoNi@C-CNB determined with TEM-EDS and ICP-OES.

Atomic %	TEM-EDS	ICP-OES
Fe	3.03	7.1
Co	2.26	6.9
Ni	7.22	19.9
S	26.1	65.9
C	33.3	--
N	20.9	--
O	7.18	--

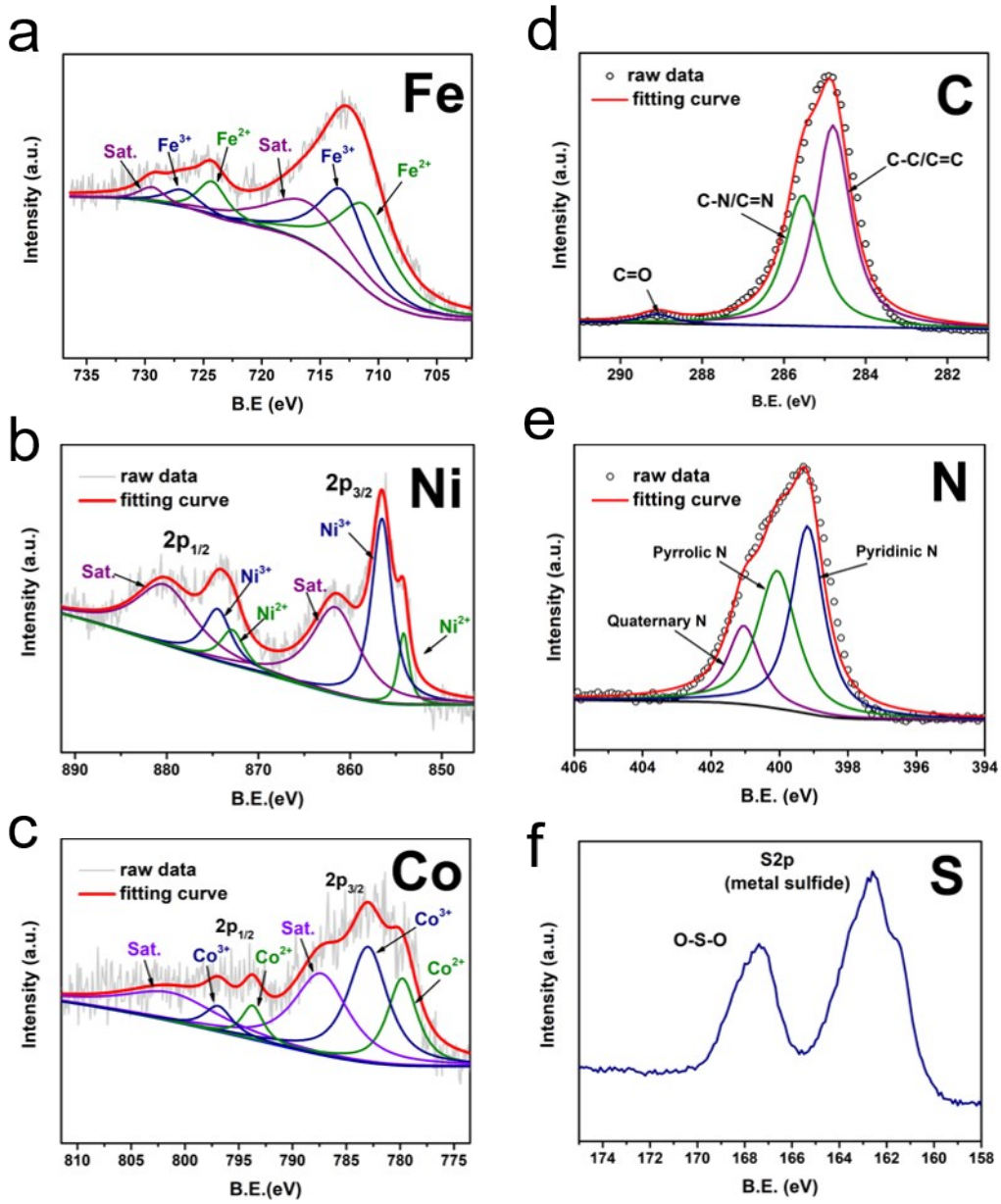

Figure S8. HRXPS patterns of (a) Fe, (b) Ni, (c) Co, (d) C, (e) N, and (f) S.

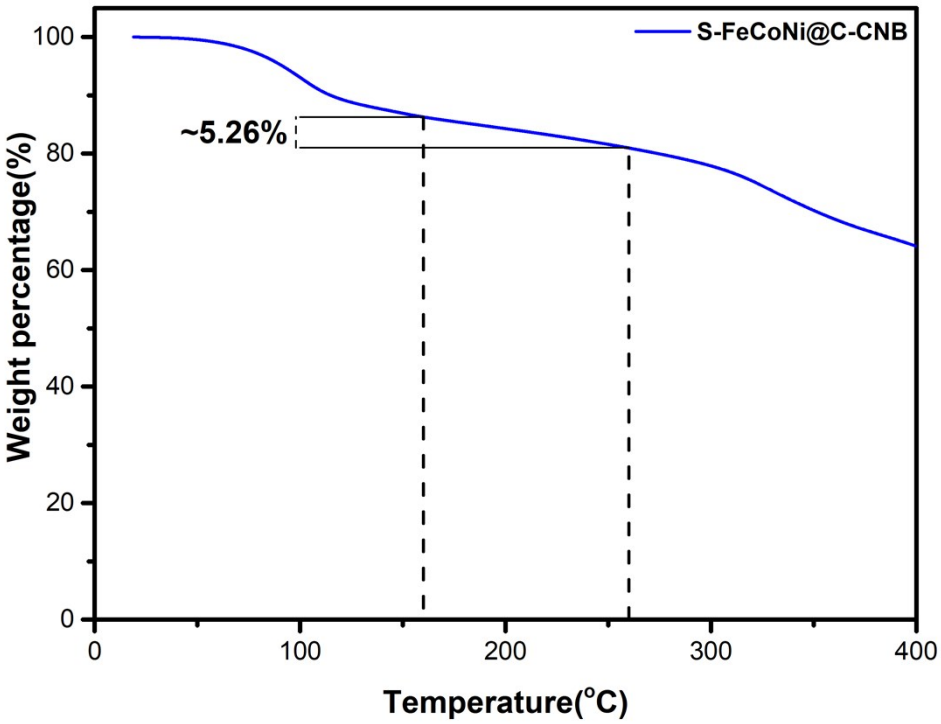

Figure S9. TG analysis of S-FeCoNi@C-CNB.

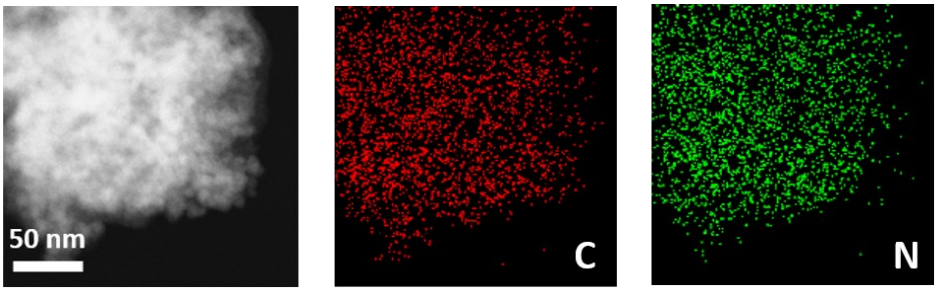

Figure S10. TEM-EDS elemental mapping of C and N in S-FeCoNi@C-CNB/S.

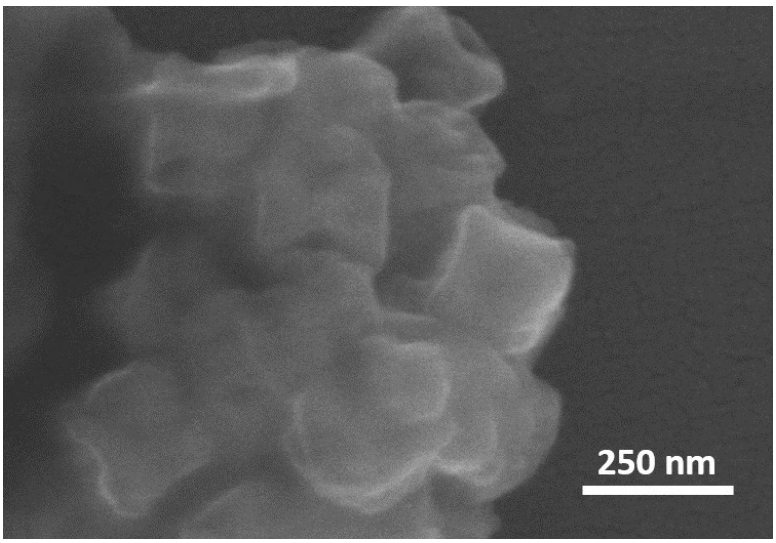

Figure S11. SEM image of S-FeCoNi@C-CNB/S after stability test.

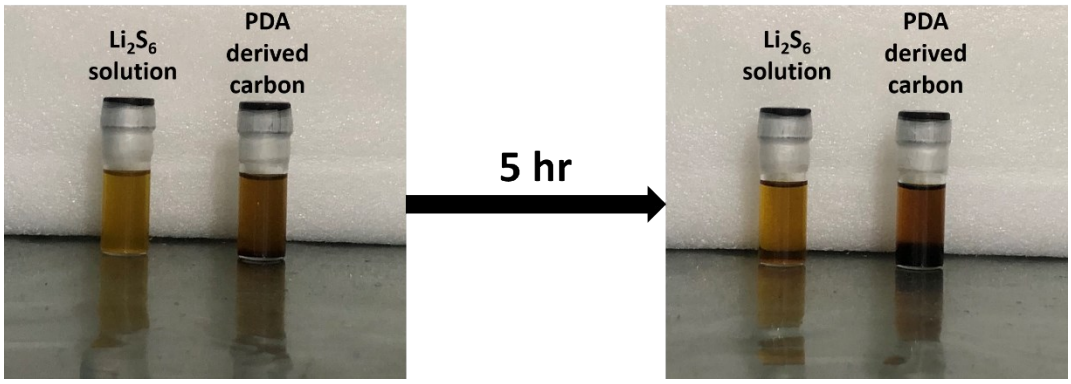

Figure S12. Results of LiPS adsorption test of PDA derived carbons.

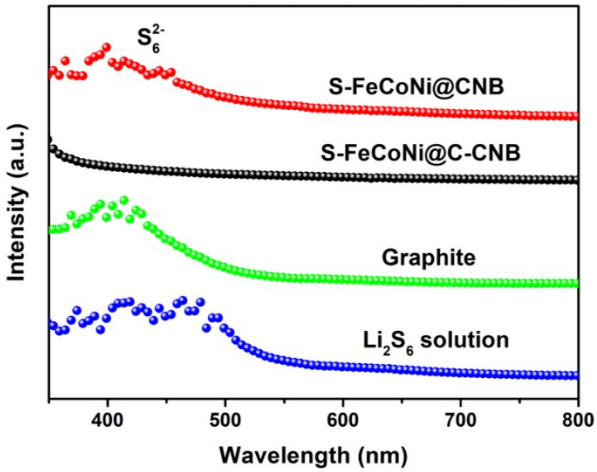

Figure S13. UV-visible spectroscopy of Li_2S_6 solutions after adsorption tests.

Table S3. Lithium ion diffusion coefficients of S-FeCoNi@C-CNB/S and S-FeCoNi@CNB/S determined based on in different reaction.

sample	Peak B' ($m^2 s^{-1}$)	Peak B ($m^2 s^{-1}$)
S-FeCoNi@C-CNB	$1.4 \times 10^{-13} \sim 1.1 \times 10^{-14}$	$1.5 \times 10^{-13} \sim 1.2 \times 10^{-14}$
S-FeCoNi@CNB	$9.0 \times 10^{-14} \sim 7.1 \times 10^{-15}$	$4.0 \times 10^{-14} \sim 3.2 \times 10^{-15}$

Table S4. Electrochemical energy storage performances of S-FeCoNi@C-CNB/S vs. recently reported state-of-the-art cathodes of LSBs.

reference	material	maximum capacity (mAh/g)	maximum C rate	cycle number	capacity decay rate (% per cycle)	sulfur content (wt%)	ratio of electrolyte to sulfur (μL/mg)
This work	**S-FeCoNi @C-CNB/S**	**1238 (0.1 C)**	**2 (655 mAh/g)**	**200 (1 C)**	**0.049**	**75**	**36**
[S1]	ZIF-67-S-PPy-60%	~990 (0.1 C)	1 (~410 mAh/g)	200 (0.1 C)	~0.3	54	26~63
[S2]	flower-like CoSP	1225 (0.1 C)	2 (606 mAh/g)	900 (1 C)	0.046	73	18
[S3]	$NiCo_2S4$@CNTs/S	780 (0.6 C)	3 (530 mAh/g)	>1000 (0.6C)	0.049	66	N/A
[S4]	HKUST-1	1377 (0.05 C)	0.6 (541 mAh/g)	300 (0.2 C)	0.06	N/A	N/A
[S5]	S/NiS@ CHS	1196 (0.1 C)	2 (674 mAh/g)	300 (0.5 C)	0.013	73.7	20
[S6]	Co_9S_8@N-CNTs	1016 (0.1 C)	2 (543 mAh/g)	300 (0.5 C)	0.1	75	N/A
[S7]	NC/MoS_3-S	1267 (0.1 C)	3 (597 mAh/g)	500 (0.5 C)	0.076	70	15
[S8]	CFS-2/CP	1500 (0.1 C)	1 (790 mAh/g)	400 (0.2 C)	0.11	70	24
[S9]	S@$Na_2Fe[Fe(CN)_6]$@PEDOT	1147 (0.2 C)	5 (683 mAh/g)	200 (2 C)	0.1	82	N/A
[S10]	S@S-ZIF-8@CNTs	1480 (0.05 C)	1 (840 mAh/g)	500 (0.1 C)	0.08	64	N/A

References:

[S1] P. Geng, S. Cao, X. Guo, J. Ding, S. Zhang, M. Zheng, H. Pang, Polypyrrole coated hollow metal–organic framework composites for lithium–sulfur batteries, Journal of Materials Chemistry A 7 (2019) 19465-19470.

[S2] X. Chen, X. Ding, H. Muheiyati, Z. Feng, L. Xu, W. Ge, Y. Qian, Hierarchical flower-like cobalt phosphosulfide derived from Prussian blue analogue as an efficient polysulfides adsorbent for long-life lithium-sulfur batteries, Nano Research 12 (2019) 1115-1120.

[S3] X. Lu, Q. Zhang, J. Wang, S. Chen, J. Ge, Z. Liu, L. Wang, H. Ding, D. Gong, H. Yang, High performance bimetal sulfides for lithium-sulfur batteries, Chemical Engineering Journal 358 (2019) 955-961.

[S4] B. Liu, R. Bo, M. Taheri, I. Di Bernardo, N. Motta, H. Chen, T. Tsuzuki, G. Yu, A. Tricoli, Metal–Organic Frameworks/Conducting Polymer Hydrogel Integrated Three-Dimensional Free-Standing Monoliths as Ultrahigh Loading Li–S Battery Electrodes, Nano letters 19 (2019) 4391-4399.

[S5] C. Ye, L. Zhang, C. Guo, D. Li, A. Vasileff, H. Wang, S.Z. Qiao, A 3D hybrid of chemically coupled nickel sulfide and hollow carbon spheres for high performance lithium–sulfur batteries, Advanced Functional Materials 27 (2017) 1702524.

[S6] Y. Xi, N. Angulakshmi, B. Zhang, X. Tian, Z. Tang, P. Xie, G.Z. Chen, Y. Zhou, A Co9S8 microsphere and N-doped carbon nanotube composite host material for lithium-sulfur batteries, Journal of Alloys and Compounds 826 (2020) 154201.

[S7] L. Guo, J. Yu, J. Xiao, A. Li, Z. Yang, L. Zeng, Q. Zhang, Y. Zhu, Enhanced Multiple Anchoring and Catalytic Conversion of Polysulfides by Amorphous MoS3 Nanoboxes for High-Performance Li-S Batteries, Angewandte Chemie International Edition (2020).

[S8] Y. Huang, D. Lv, Z. Zhang, Y. Ding, F. Lai, Q. Wu, H. Wang, Q. Li, Y. Cai, Z. Ma, Co-Fe Bimetallic sulfide with Strengthened Chemical Adsorption and Catalytic Activity for Polysulfides in Lithium-Sulfur Batteries, Chemical Engineering Journal (2020) 124122.

[S9] D. Su, M. Cortie, H. Fan, G. Wang, Prussian Blue Nanocubes with an Open Framework Structure Coated with PEDOT as High-Capacity Cathodes for Lithium–Sulfur Batteries, Advanced Materials 29 (2017) 1700587.

[S10] H. Zhang, W. Zhao, M. Zou, Y. Wang, Y. Chen, L. Xu, H. Wu, A. Cao, 3D, Mutually embedded MOF@ carbon nanotube hybrid networks for high-performance lithium-sulfur batteries, Advanced Energy Materials 8 (2018) 1800013.